Nuclear Materials and Energy 48 (2026) 102190

Contents lists available at ScienceDirect

Nuclear Materials and Energy

journal homepage: www.elsevier.com/locate/nme

Development and validation of an oscillating energy degrader and dose gradient system for ion irradiation of fusion materials☆

Mario Matić[a], Toni Dunatov[a], Tonči Tadić[a,*], Dmitry Terentyev[b,c], Koray L. Iroc[b], Tatjana Filipič[d], Janez Kovač[d]

[a] Ruđer Bošković Institute, Bijenička cesta 54, 10000 Zagreb, Croatia
[b] SCK CEN, The Belgian Nuclear Research Centre, Boeretang 200, 2400 Mol, Belgium
[c] Department of Materials, Textiles and Chemical Engineering, Ghent University, Belgium
[d] Jožef Stefan Institute, Jamova cesta 39, 1000 Ljubljana, Slovenia

ARTICLE INFO

Keywords:
Ion irradiation
Fusion reactor materials
Eurofer
Helium
Energy degrader
Dose gradient
TEM
SIMS

ABSTRACT

Ion irradiation is widely used to emulate neutron-induced damage and transmutation effects in fusion reactor materials. Heavy ions generate displacement damage over a micrometer-scale depth range preceding their implantation peak, where the damage level remains relatively uniform. Light ions such as helium and hydrogen are introduced to simulate gas production originating from (n,α) and (n,p) nuclear reactions. Accurate emulation of fusion conditions therefore requires a homogeneous distribution of light ions throughout the uniform portion of the damage region created by heavy ions. However, the inherently narrow implantation range of light ions, typically limited to a few hundred nanometers, makes achieving uniform gas concentrations across the full micrometer-scale damaged volume challenging.

In this work, we report the development of two experimental techniques at the DiFU dual-beam facility designed to improve irradiation efficiency: (i) an oscillating aluminum energy degrader that broadens the light-ion implantation profile over approximately one micrometer while maintaining depth homogeneity, and (ii) an electrostatic beam scanning dose gradient system that enables multiple implantation doses on a single specimen in a single irradiation run. For the validation case, helium ions were implanted into Eurofer97 steel using the energy degrader and validated by transmission electron microscopy (TEM) after in situ heating, revealing a helium bubble distribution consistent with the predicted broadened implantation range. Lithium implantation was used as a surrogate to validate the dose gradient concept by time-of-flight secondary ion mass spectrometry (ToF-SIMS), confirming a linear dose ratio across the irradiated surface. The use of an oscillating energy degrader and dose gradients significantly enhances experimental efficiency and reproducibility for fusion materials irradiation studies.

1. Introduction

Neutron irradiation in fusion environments degrades materials through two concurrent mechanisms. Displacement damage is produced by elastic collisions between fast neutrons and lattice atoms, leading to the formation of point defects and defect clusters distributed over relatively large depths. Transmutation products are generated through nuclear reactions, most notably (n,α) and (n,p) reactions, resulting in the continuous production of helium and hydrogen nuclei within the material. Helium poses a greater challenge because of its low solubility and diffusivity compared to hydrogen, which allows it to accumulate and remain trapped at defects. Helium strongly influences microstructural evolution by stabilizing vacancy clusters, promoting bubble formation, and enhancing swelling and embrittlement. Accurate experimental simulation of fusion conditions therefore requires the simultaneous reproduction of both neutron-induced displacement damage and helium production within the same material volume. Since producing fusion-relevant doses in high-flux fission reactors is limited, expensive and time consuming, and relevant fusion neutron sources such as IFMIF-DONES are still under development, ion irradiation has become a

☆ This article is part of a special issue entitled: 'ICFRM-22' published in Nuclear Materials and Energy.

* Corresponding author.
E-mail address: tonci.tadic@irb.hr (T. Tadić).

https://doi.org/10.1016/j.nme.2026.102190
Received 30 January 2026; Received in revised form 6 July 2026; Accepted 14 July 2026
Available online 15 July 2026

widely adopted surrogate technique for studying radiation effects in fusion materials [1,2].

Ion implantation allows controlled introduction of displacement damage using heavy ions and simulation of transmutation products using light ions, primarily helium and hydrogen [1]. While heavy-ion irradiation produces relatively broad damage profiles extending over a micrometer prior to the ion range peak, light ions stop within a narrow depth interval of a few hundred nanometers. As a result, gas-related effects are confined to a limited region, biasing microstructural evolution toward the implantation peak rather than the uniformly damaged bulk.

To address these limitations, two experimental approaches were developed and implemented at the DiFU dual-beam irradiation facility at the Ruđer Bošković Institute (RBI) in Zagreb, Croatia [3]: an oscillating energy degrader system that broadens the implantation depth of light ions, and a dose gradient system based on an electrostatic beam scanning system that enables multiple doses on a single sample per one irradiation run. The primary objective of this work is to describe the design and implementation of these two systems.

2. Ion implantation for fusion materials

Ion implantation offers precise control over irradiation parameters such as ion species, energy, fluence, and temperature, and is therefore widely used to study radiation effects in fusion materials. In accelerator-based simulations, heavy ions are used to generate displacement damage, while light ions are implanted to reproduce the production and accumulation of transmutation gases. Dual ion beam irradiation is a specific use case where both are applied at the same time to more realistically reproduce fusion irradiation conditions.

For both heavy and light ions, the irradiation process results in a characteristic depth-dependent response: a relatively broad region of displacement damage extending ahead of the ion range peak, followed by a narrow implantation zone where ions come to rest. The width of the damage region is governed primarily by the ion energy and mass, whereas the implantation peak remains confined to a comparatively small depth interval. Upon concurrent or subsequent thermal treatment relative to irradiation, implanted helium becomes mobile and agglomerates into nanoscale bubbles, as observed by transmission electron microscopy (see Fig. 1).

In the case of heavy-ion irradiation, experimental studies typically focus on the damage region preceding the implantation peak, where the damage level is relatively uniform over micrometer-scale depths. This region is well suited for microstructural and mechanical characterization and serves as a proxy for neutron-induced displacement damage. For light ions such as helium and hydrogen, the region of interest is instead the implantation zone itself, as this is where transmutation gases accumulate. However, at a fixed implantation energy, the width of the stopping range of light ions is limited to only about 100 nm. When gas implantation is required within the damage region created by heavy ions, this narrow implantation width severely restricts the accessible analysis volume and leads to a concentration of gas-related effects near the end-of-range region. Fig. 2 shows the implantation depth profile of 400 keV He ions together with the displacement damage profile produced by 10 MeV Fe ions in FeCr steel. While the He implantation is positioned within the relatively uniform damage region, its concentration is confined to a narrow peak when a single implantation energy is used.

One approach to extending the implantation depth of light ions is the use of multiple discrete implantation energies. While this can increase the overall implantation region, it results in a superposition of implantation peaks rather than a continuous and uniform distribution, and it is experimentally inefficient due to the need for frequent changes of accelerator settings. A more effective solution is the use of an energy degrader, made of thin foils which the beam can penetrate and placed in the beam path before the target. By imposing a controlled and continuously varying energy loss, the degrader allows light ions to reach the sample with a continuous range of energies, thereby broadening the implantation region homogeneously. When properly configured, this approach enables light ions to be distributed across the full damage region generated by heavy ions, without repeated adjustments of the accelerator parameters.

Conventional rotating wheel degraders [4,5] introduce several technical constraints. The discrete nature of the mounted foils produces a superposition of distinct peaks rather than a homogenous profile. The mechanical gaps between foils cause beam chopping, which reduces the total implanted fluence. Standard rotating systems also provide a fixed dwell time for each foil thickness, although thicker foils induce more lateral scattering.

An oscillating degrader addresses these limitations by utilizing a wedge with a continuously variable thickness profile. Modulating the oscillation velocity allows for precise compensation of scattering losses, ultimately ensuring a truly uniform dose distribution across the entire implantation depth [6,7]. Fig. 3 shows an idealized simulation of the 1.3

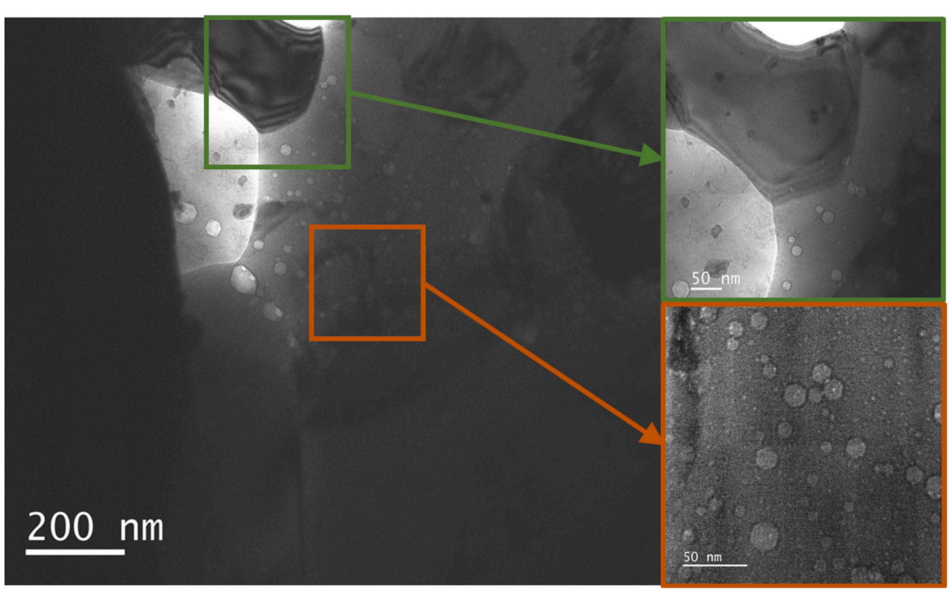

Fig. 1. In situ TEM image of Eurofer97 irradiated with helium and heated to 700 °C, showing the formation and evolution of helium bubbles.

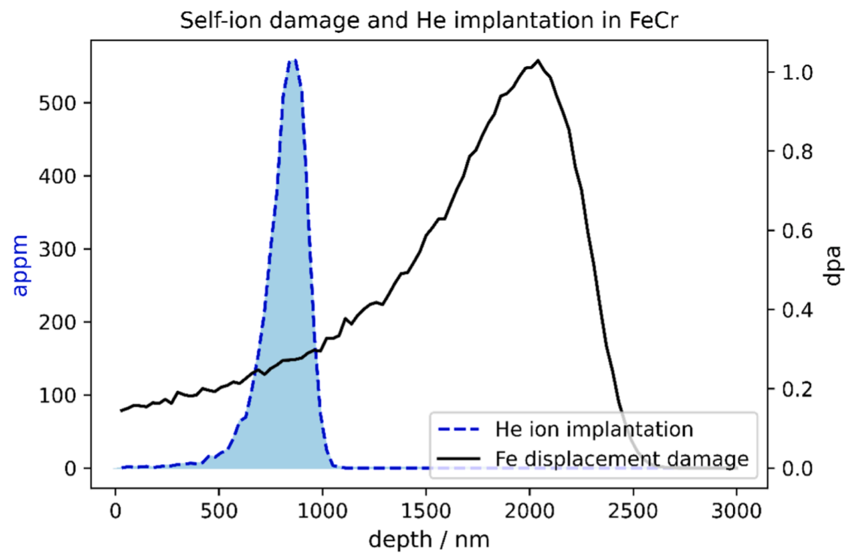

Fig. 2. The implantation profile of 0.4 MeV He in FeCr compared to the damage profile of 10 MeV Fe. It is seen that the damage profile is significantly wider.

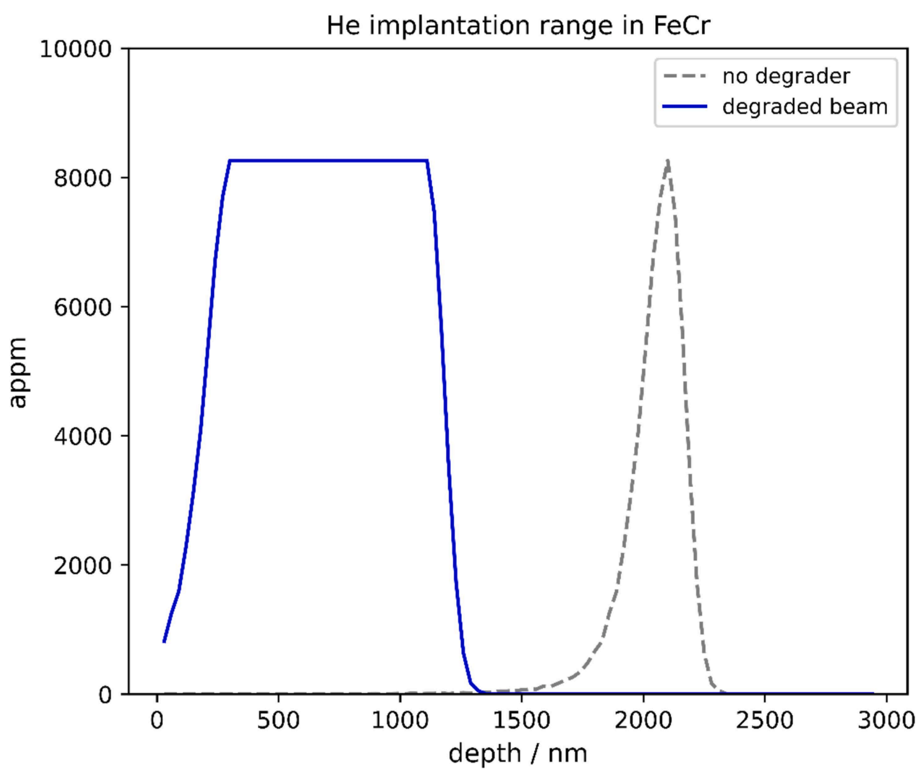

Fig. 3. Comparison of the implantation profile of 1.3 MeV He beam, without a degrader, and after passage through the oscillating degrader. This simulation serves as the theoretical objective for achieving a broadened and uniform implantation profile. The implantation range of a degraded beam is larger by a factor of approximately 4.

MeV He depth profile implanted in FeCr steel, comparing the single-energy implantation with the theoretical target profile achieved using the 1.8 µm Al foil oscillating degrader. The simulation represents the intended broadened profile and serves as a theoretical objective based on fixed ion ranges and a homogeneous medium.

3. Oscillating energy degrader

3.1. Principle of operation

The energy degrader consists of an aluminum foil mounted on a frame that oscillates in front of the ion beam. When the foil is perpendicular to the beam (0° position), ions traverse the nominal foil thickness *d*. As the foil tilts by an angle θ around a pivot point, the effective thickness increases according to d/cos(θ). At the maximum oscillation angle of 60°, the effective thickness reaches *2d*. The initial beam energy E_0 is selected based on the specific capabilities of the ion accelerator and the required implantation range. By selecting an initial ion energy sufficiently high to allow penetration through the maximum effective thickness *2d*, the oscillating degrader produces a continuous spectrum of ion energies such that the ion range swifts between depths corresponding to foil thicknesses *d* and *2d*. Consequently, ions are implanted over a broad depth interval within the target material that could extend up to a micrometer, as shown in Fig. 4.

3.2. Linearity correction

If the degrader were to oscillate with a constant angular velocity around the pivotal point, the resulting implantation profile would be strongly non-uniform. This arises from the cosine dependence of the effective thickness: equal angular increments correspond to small changes in effective thickness near the 0° position, but much larger changes near the 60° position. As a result, a constant-speed oscillation would bias the implanted dose toward deeper regions corresponding to lower effective thickness. To achieve a more uniform implantation, the oscillation motion must be non-linear. Specifically, the degrader must move faster near the 0° position and progressively slower as it approaches the maximum 60° angle. This ensures that each effective thickness interval, and therefore each implantation depth, receives an equal fraction of the total fluence. In practice, this correction is implemented by programming the stepper motor controlling the degrader to follow a cosine-dependent angular velocity profile.

3.3. Multiple scattering correction

A second source of non-uniformity arises from multiple scattering of ions within the degrader foil. As the effective thickness increases with angle, ions experience increased scattering, leading to beam broadening and a reduction in the number of ions reaching the intended irradiation area on the sample. Consequently, implantation at larger angles (shallower depths) would receive a lower effective dose compared to implantation at smaller angles, which again biases the dose toward deeper regions. The implanted He depth profile shown in Fig. 5 illustrates how the He distribution becomes more uniform when both corrections are implemented.

To compensate for this effect, ion scattering angle as a function of foil thickness is modeled using reduced variables to characterize the angular distribution spread [8,9]. The angular spread is quantified by the reduced half-width at half-maximum (HWHM), α^*, which relates to the physical scattering angle (α) and the ion energy (E) through the expression:

$$\alpha^* = \frac{Ea}{2Z_1Z_2e^2}\alpha, \tag{1}$$

where Z_1 and Z_2 are the atomic numbers of the ion and target, e is the elementary charge, and a is the screening radius. This spread is a function of the reduced foil thickness τ, defined as:

$$\tau = \pi a^2 N x, \tag{2}$$

where N is the atomic density and x is the foil thickness [8]. For the thicknesses and energies used, the distribution $f(\tau, \alpha^*)$ is typically modeled as a linear combination of Gaussian and Lorentzian functions to accurately represent both the central peak and the multiple-scattering tails [10].

A Python script was developed to quantify the beam loss as a function of the foil tilt angle θ. The initial ion beam is modeled with a rectangular intensity profile of width $w = 5$mm. For each effective thickness $x = d(\theta)$, the script calculates the angular distribution spread $f(\tau, \alpha^*)$ and convolves it with the initial beam profile. To determine the beam loss, both the initial rectangular profile and the broadened profile are normalized to an area of 1. The fraction of the beam remaining within the intended 5 mm irradiation zone is calculated as the overlap integral between the two profiles. The beam loss is then defined as the fraction of the distribution falling outside the target width. To ensure a uniform final dose, the dwell time at each tilt angle is multiplied by a compensation factor. This adjusted timing is integrated into the final velocity profile executed by the stepper motor, effectively increasing the implantation time at larger angles where scattering losses are most significant.

For implementation under new irradiation conditions, the calibration procedure consists of: (i) selecting an initial ion energy sufficient for ions to traverse the maximum effective foil thickness while maintaining implantation within the targeted damage region; (ii) calculating the geometric correction associated with the $d/\cos(\theta)$ dependence of the effective foil thickness; (iii) estimating scattering-induced beam losses as a function of tilt angle; and (iv) generating the compensated dwell-time

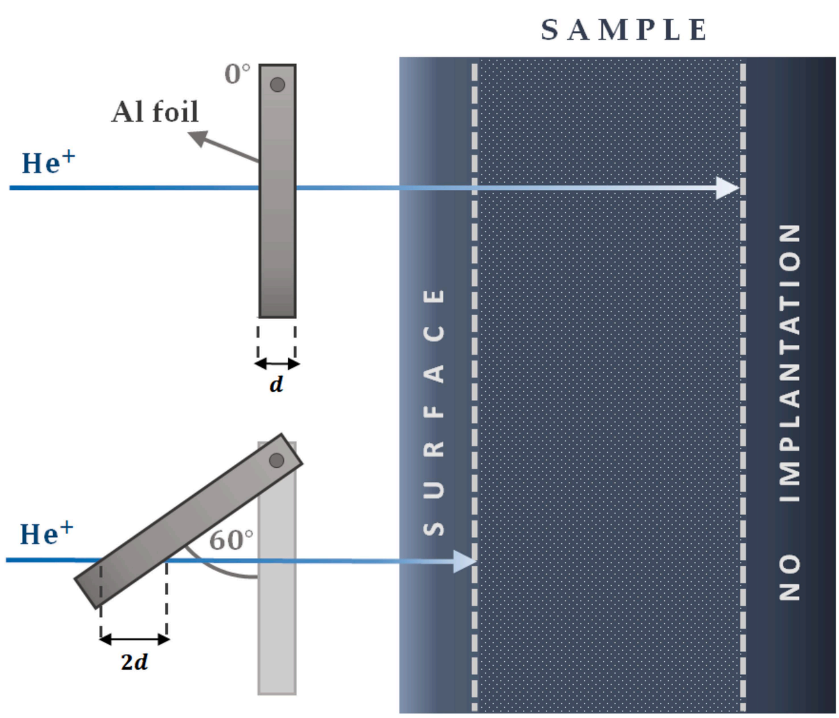

Fig. 4. Schematic of the working principle of the degrader.

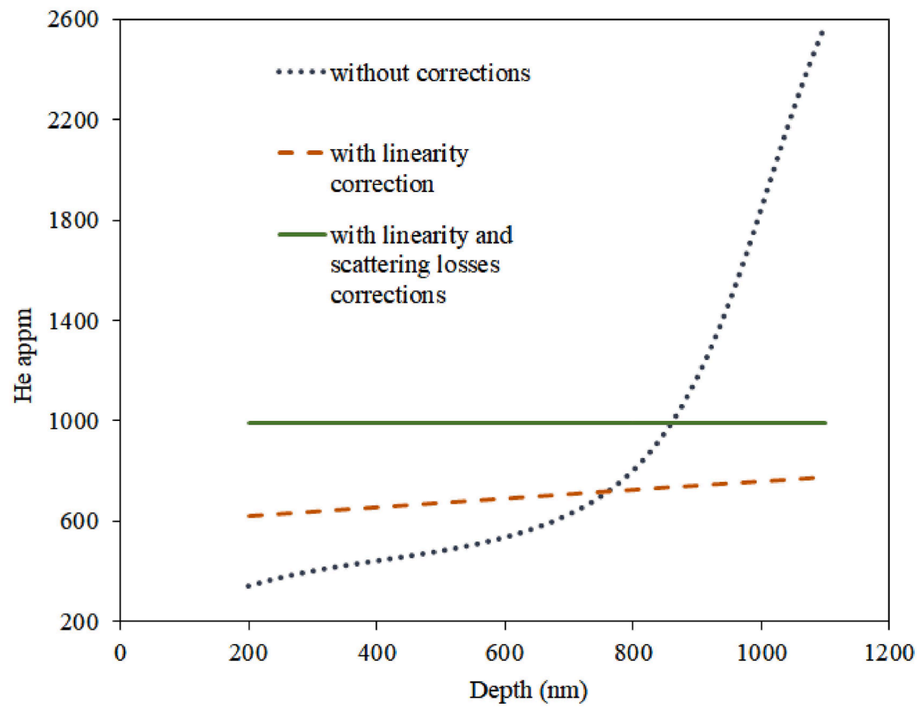

Fig. 5. Implanted 1.3 MeV He^+ depth profile when implanted in Eurofer97 with an oscillating degrader: without any corrections; with only the linearity correction; and with both linearity and multiple scattering corrections.

profile executed by the stepper motor during irradiation.

By combining the linearity correction and the scattering-loss correction, the complete oscillation scheme is executed via a stepper motor during irradiation and a broadened implantation profile over a micrometer-scale depth range is achieved.

4. Dose gradient system

4.1. Motivation

Irradiation experiments often require multiple doses to investigate dose-dependent phenomena. Usually, this requires multiple samples and repeated irradiation runs, which is time-consuming and introduces uncertainties due to variations in temperature, vacuum conditions, and dose rate between different runs of experiment. Post-irradiation analysis typically probes only a small fraction of the irradiated area, and therefore one sample could easily fit multiple doses. Ideally, a dose gradient can be established across the irradiation area, allowing analysis of multiple different doses per sample.

4.2. Electrostatic scanning concept

The dose gradient system addresses these challenges by generating a controlled, linear dose variation across a single sample during one irradiation run. Two electrostatic scanners, oriented horizontally and vertically along the beamline, deflect the ion beam using strong electric fields. While scanners are commonly used for beam alignment and homogenization, a tailored scanning program allows the beam to be distributed non-uniformly by varying the dwell time per point, producing a linear dose gradient (Fig. 6). The gradient can be oriented

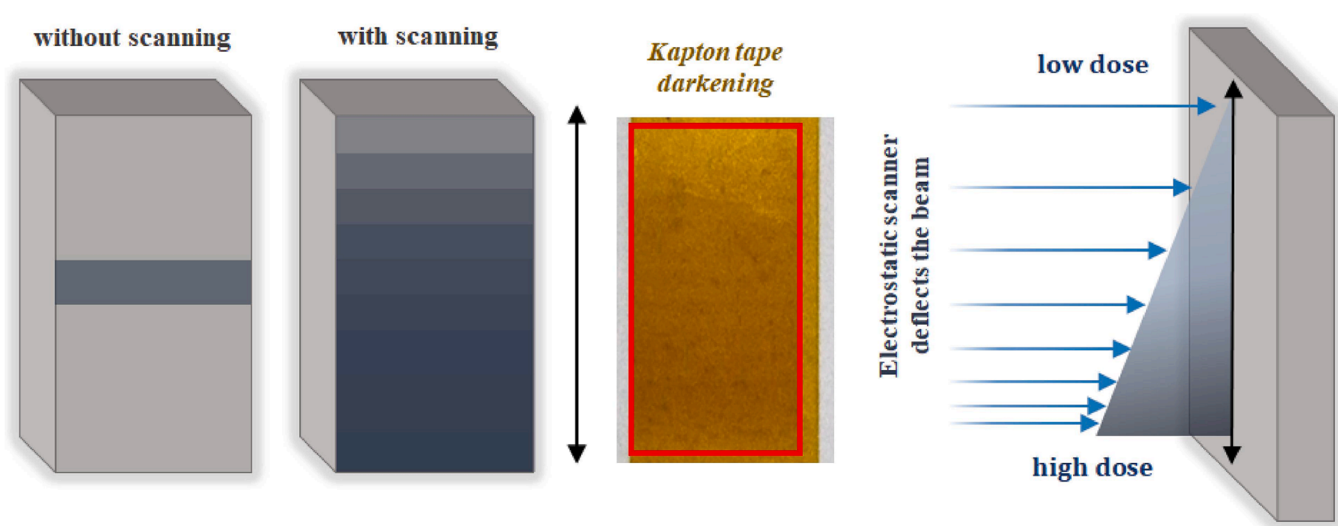

Fig. 6. Schematic of the working principle of the dose gradient.

horizontally, vertically, or diagonally, and the dose ratio between two edge points of the irradiated area can be precisely adjusted. This approach enables multiple doses to be realized on a single specimen under identical irradiation conditions, significantly improving experimental efficiency and reproducibility.

5. Experimental procedure

5.1. Materials and irradiation conditions

All irradiations were performed in the DiFU chamber at RBI. Eurofer97 (batch 2) steel samples with dimensions of 10 mm × 10 mm × 1.5 mm and 20 mm × 10 mm × 1.5 mm were mechanically polished prior to irradiation at KIT, Karlsruhe, Germany. Experiments were conducted at room temperature, and the base pressure during irradiation was on the order of 10^{-8} mbar.

For energy degrader validation, 1.3 MeV He^{+} ions were implanted into Eurofer97 to a total incident fluence of $4{\cdot}10^{16}$ He/cm^2 using an oscillating aluminum foil with a nominal thickness of 1.8 µm mounted on the degrader frame (Fig. 7). Due to multiple scattering in the degrader, the effective implanted fluence in the sample is lower than the incident value. The degrader was positioned 4 cm in front of the sample in the 0° configuration, and during irradiation it oscillated between the 0° and 60° position. A 5 × 5 mm^2 area was irradiated to a nominal concentration of approximately 1000 appm He. According to SRIM [11] simulations, the expected implantation range extended from roughly 200 nm to 1200 nm. The mechanical oscillation of the foil is driven by a VEXTA 2-phase stepper motor (Model 3167–9012) with a native resolution of 1.8° per step. The motor is interfaced with an X-NUCLEO-IHM02A1 expansion board (based on the L6470 driver). The entire system is managed by a custom control application developed in C# enabling precise stepping and velocity modulation. For the validation experiments described in this work, a total oscillation period of 60 s was used for one full cycle (0°-60°-0°).

For dose gradient validation, 1.4 MeV Li^{2+} ions were implanted into Eurofer97 to a total fluence of $1.7{\cdot}10^{15}$ Li/cm^2 using a programmed linear gradient with a dose ratio of 1:4 across a length of approximately 1.5 cm. The dose gradient is generated using two pairs of Danfysik electrostatic scanners. The plates are 250 mm in length with a 30 mm separation, capable of a maximum deflection of ±20 mm at the sample position with a maximum voltage difference of ±10 kV. High-voltage modulation is provided by Matsusada 10B10 high-frequency amplifiers, controlled by a dedicated RBI Scanning Control Card and custom synchronization software. The system supports a scanning pattern with a minimum of 10 positions per axis and a dwell time as low as 10 µs, allowing for a maximum scanning frequency of 10 kHz. For the dose gradient validation using 1.4 MeV Li^{2+} ions, a linear gradient was programmed across a 1.5 cm width using 15 discrete scanning points. To achieve the 1:4 dose ratio, the dwell time was modulated from 10 µs at the low-dose end to 40 µs at the high-dose end. By gradually increasing the dwell time at each position across the horizontal axis, a linear dose gradient was established while maintaining identical vacuum and temperature conditions across the entire specimen. Irradiation area was 10 × 15 mm^2. Lithium was selected as a surrogate for helium because, unlike helium [12], it is readily detected by SIMS, and unlike hydrogen, it is not present as a background species in vacuum systems.

5.2. TEM and SIMS analysis

To characterize the helium implantation profile, focused ion beam (FIB) milling was used to prepare a cross-sectional lamella approximately 90 nm thick from the irradiated region. TEM analysis was performed by JEOL JEM-ARM300F2 TEM equipped with a cold field emission gun as electron source, operating at 300 kV at SCK CEN (Mol, Belgium). The lamella was heated in situ up to 700 °C to promote helium bubble formation. The nature of the observed features was confirmed by their visibility at overfocused and underfocused imaging conditions (±2µm), verifying their identification as voids.

To quantitatively validate the dose gradient, ToF-SIMS depth profiling was carried out at the Department of Surface Engineering, Jožef Stefan Institute (JSI), Ljubljana. Three positions along the dose gradient were selected for analysis, corresponding nominally to approximately 1000 appm (low-dose end), 2000 appm (central region), and 3000 appm (high-dose end). SIMS measurements were performed using a Bi^{+} primary ion beam operated at 30 keV with a beam current of 0.8 pA and a probe diameter of approximately 5 µm. The analysis area was 100 × 100 µm^2. Sputtering was achieved using a Cs^{+} beam at 2 keV, rastered over an area of 300 × 300 µm^2, resulting in an estimated sputter rate of 0.38 nm/s. Positive secondary ions in the mass range from 0 to 250 Da were collected. Measurements were performed using a ToF-SIMS 5 instrument (IONTOF, Germany). Lithium depth profiles were normalized to the iron signal to account for possible variations in sputter yield and instrumental sensitivity. The resulting profiles enabled a direct comparison of relative lithium concentrations between the three

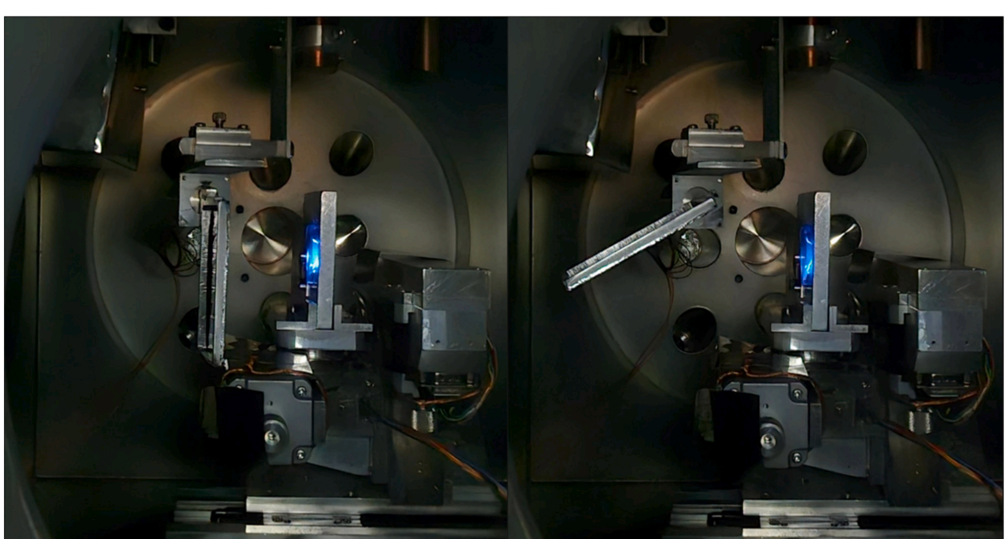

Fig. 7. Oscillating degrader in the DiFU chamber. On the sample holder, the quartz glass exhibits beam-induced luminescence as the beam passes through the foil at the 0° and 60° positions.

analyzed positions.

6. Results

6.1. Helium implantation profile characterized by TEM

Cross-sectional transmission electron microscopy was used to investigate the depth distribution of helium in Eurofer97 after implantation using the oscillating energy degrader. Following focused ion beam preparation, the lamella was examined in the as-prepared state and subsequently during in situ heating. Prior to heating, no clear contrast associated with helium was observed, which is consistent with helium being present in a dispersed atomic state. Upon heating to 700 °C, a population of nanoscale cavities became visible within the ferritic–martensitic matrix. The cavities exhibited characteristic Fresnel contrast, appearing bright under underfocused conditions and dark under overfocused conditions, confirming their identification as voids associated with helium bubble formation.

A TEM image of the depth profile at −1.5 μm underfocused condition is shown in Fig. 8. Fig. 8a is intended to provide context for the exact positions of the higher-magnification insets (8b and 8c) and is annotated with dashed lines to indicate the implantation zone. While individual bubbles are difficult to discern in the overview image due to thickness gradients and diffraction contrast, the high-contrast insets provide the necessary clarity to verify bubble morphology at the surface and end-of-range, respectively.

To confirm the implantation boundaries, a systematic Fresnel contrast analysis was performed across the entire depth of the lamella. While nanoscale cavities were clearly identified via the bright/dark contrast shift in the 200–1200 nm range, no such features were observed in the near-surface region (<200 nm) or in the bulk region beyond 1200 nm. Within this interval, the bubble density was relatively uniform, with no pronounced maximum corresponding to a single implantation energy. The termination at 1200 nm is consistent with the physical limits of ion penetration predicted by SRIM.

The experimentally observed depth range and uniformity of the bubble distribution are in good agreement with SRIM simulations for 1.3 MeV He^{+} ions implanted using the oscillating 1.8 μm aluminum degrader into Eurofer97. These observations confirm that the degrader, together with the implemented linearity and scattering corrections, successfully produced a broadened and approximately uniform helium implantation depth profile.

A TEM micrograph covering an approximately 1 μm wide region containing helium bubbles was divided into several equally sized sub-regions to account for local variations in brightness and contrast caused by different grain orientations and thickness conditions. Background subtraction and thresholding were performed separately in ImageJ for each sub-region, with threshold values manually adjusted to selectively identify features corresponding to helium bubbles. The processed image was subsequently divided into 100 nm wide columns, and the total segmented bubble area within each column was summed in relative units to obtain the depth-dependent bubble area distribution profile shown in Fig. 9. The total bubble area serves as a proxy for the total helium sequestration at each depth interval.

6.2. Validation of dose gradient by SIMS

SIMS depth profiles obtained from the three selected positions along the lithium-implanted sample showed similar implantation depth distributions, indicating consistent implantation geometry and beam

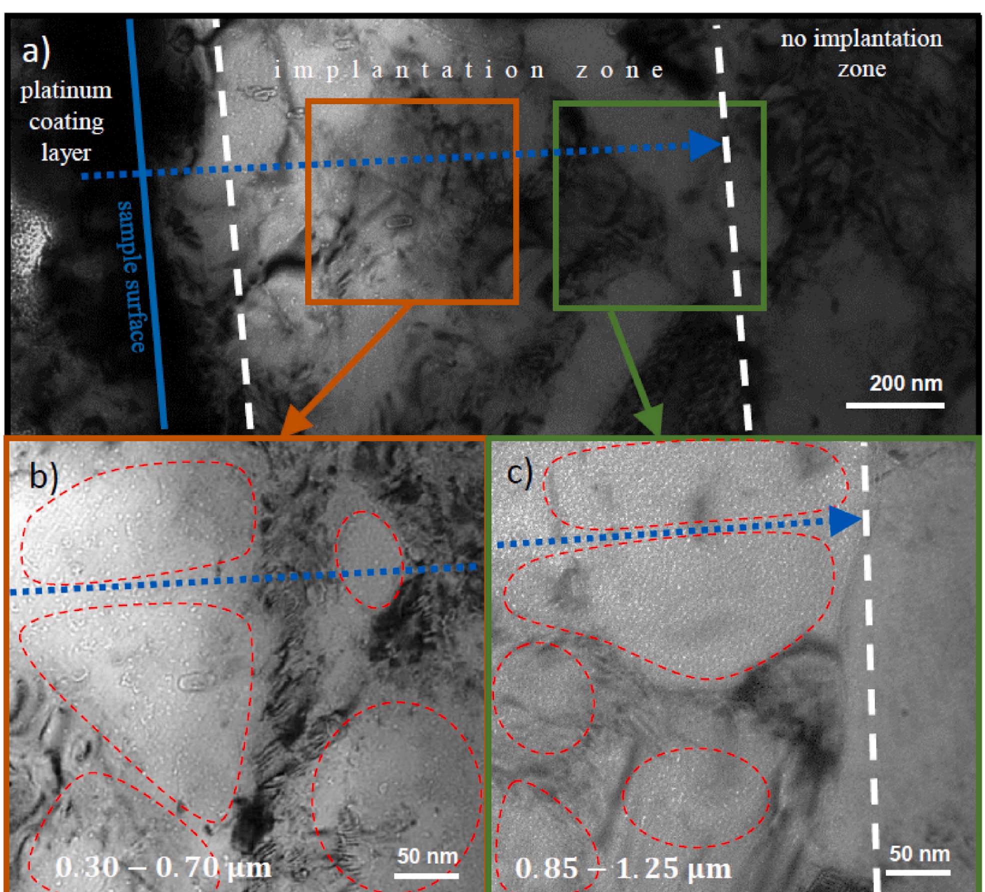

Fig. 8. Bright-field TEM image of depth profile at −1.5 μm underfocused condition.

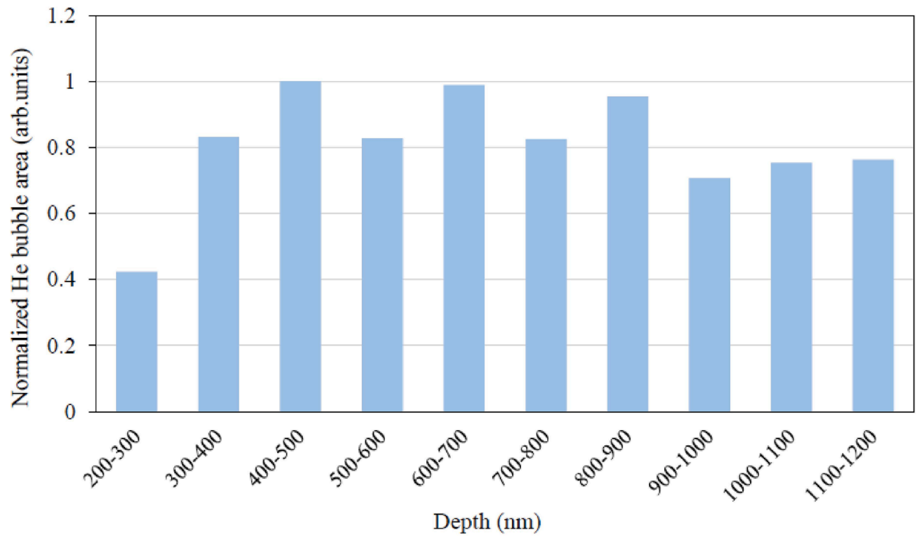

Fig. 9. Normalized bubble area distribution as a function of depth, obtained from segmented TEM micrograph. The histogram represents summed bubble area within 100 nm columns in the implanted region. This distribution serves as a representative proxy for the relative helium concentration profile.

conditions across the irradiated area. In contrast, the absolute lithium signal intensities varied systematically between the three locations.

When the lithium signals were normalized to iron and plotted together (Fig. 10), the relative peak concentrations followed a clear raw ratio of 0.0560: 0.153: 0.226, or approximately 1:2.5:4 for the low-, medium-, and high-dose positions, respectively. This ratio closely matches the programmed linear dose gradient and demonstrates that the electrostatic scanning system reliably generated a linear variation in implanted dose across the sample surface.

The good agreement between the intended and measured dose ratios indicates stable beam deflection, accurate gradient control, and reproducible scanning conditions throughout the irradiation. These results confirm that lithium implantation provides a robust and quantitative means of validating dose gradients intended for helium implantation, for which SIMS sensitivity is inherently limited.

7. Discussion

The results presented in this work demonstrate that the oscillating energy degrader effectively overcomes the intrinsic limitation of narrow light-ion implantation profiles. By dynamically varying the effective foil thickness and correcting for both geometric non-linearity and multiple scattering losses, a helium implantation profile spanning approximately one micrometer was achieved. This depth range overlaps well with the region of interest in heavy-ion irradiations, where displacement damage is relatively uniform, and thus enables more realistic emulation of fusion-relevant irradiation conditions. The use of an oscillating energy degrader provides a significant advantage over conventional rotating wheel systems [4,5]. While rotating wheels rely on a series of discrete foil thicknesses, which result in a discontinuous implantation profile composed of separate peaks, the continuous angular modulation used here ensures a smooth distribution of ion energies.

The TEM observations provide direct microstructural validation of the degrader concept. The absence of a pronounced bubble density peak and the relatively uniform distribution of helium bubbles across the implanted region indicate that the time-dependent modulation of the degrader angle successfully compensated for the cosine dependence of effective thickness. Without this correction, implantation would be strongly biased toward deeper regions corresponding to smaller angles. Additionally, the correction for scattering losses at larger angles proved

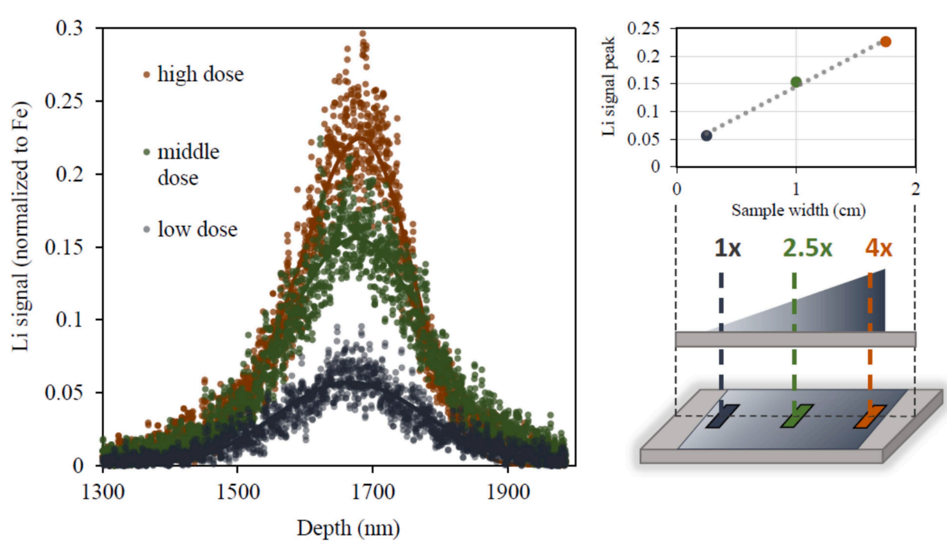

Fig. 10. SIMS depth profiling of 1.4 MeV Li^{2+} implanted in Eurofer97 with a lateral dose gradient. Lithium signal (normalized to Fe) is shown as a function of depth for three locations corresponding to low, middle, and high implantation doses.

essential for avoiding further bias toward deeper implantation depths. It is important to note that the TEM-observed bubble distribution is the result of both the initial implantation profile and subsequent thermal evolution at 700 °C. At this temperature, helium is highly mobile and traps at radiation-induced defects, eventually forming bubbles. While the final bubble density and size are governed by diffusion-to-sink kinetics, the fact that the observedbubbles are distributed across a 1000 nm zone without a dominant cluster at any single depth confirms that the helium was initially introduced into a broad volume. The depth-dependent fluctuations in the observed implantation area are attributed to the stochastic nature of ion penetration and bubble nucleation within the relatively small sampling volume of a TEM lamella. Furthermore, local microstructural features, such as grain orientation and variations in lamella thickness and temperature, may locally influence bubble growth. Additionally, the boundaries of the implantation zone are not expected to be perfectly sharp due to diffusion effects that naturally broaden the edges of the sequestered helium profile. Our primary objective was to characterize the helium sequestration profile using the total projected bubble area as a representative proxy for helium concentration. We prioritized the integral gas accumulation over individual bubble distribution characteristics, as the goal of the oscillating degrader and the corrections is to achieve a uniform volumetric concentration of helium. In this context, the total volume fraction serves as the most direct indicator of the quantity of sequestered helium per depth interval.

The dose gradient system complements the energy degrader by enabling efficient dose-dependent studies. Producing multiple doses on a single specimen during a single irradiation run eliminates the need for multiple samples and ensures identical irradiation conditions for all doses [13]. This is particularly advantageous for post-irradiation characterization techniques that probe only a limited area of the sample, such as TEM or nanoindentation.

The successful SIMS validation confirms that the dose gradient is linear, reproducible, and quantitatively well controlled. While helium itself is challenging to quantify by SIMS, the demonstrated lithium-based validation provides confidence that the same approach can be applied to helium and hydrogen implantations, provided that suitable surrogate ions or complementary characterization techniques are used. While Li ions exhibit higher lateral straggling than He at these energies, SRIM calculations confirm that the straggling remains on the micrometer scale. This is negligible relative to the 5 mm beam width and 15 mm scan length, ensuring that the gradient linearity is preserved across the analysis region. Given the low beam currents used ($< 1\mu A$) and the high thermal conductivity of the approximately 1 mm-thick substrate, the temperature rise due to the ion beam is negligible. Furthermore, the high scanning frequency (up to 10 kHz) effectively distributes the beam power almost instantaneously across the surface, mitigating the risk of differential heating between the high-dose and low-dose regions. This ensures that the observed dose-dependent phenomena are a result of ion fluence variations rather than localized temperature fluctuations across the sample surface.

While these techniques significantly improve the fidelity of ion-beam simulations, it must be acknowledged that ion implantation remains an engineering approximation of the fusion environment. Unlike neutron-induced transmutation, which generates helium and hydrogen continuously within the bulk material, ion implantation is an externally driven process. However, by broadening the implantation profile and controlling the dose gradient, the experimental conditions approach a state that more closely mimics the physical reality of continuous gas production in fusion reactor components.

8. Conclusions

An oscillating aluminum energy degrader and an electrostatic dose gradient system were successfully applied to light-ion implantation in Eurofer97 steel. TEM analysis confirmed a broadened helium implantation profile spanning approximately 1000 nm in depth, demonstrating that the intended level of homogeneity was achieved despite the statistical fluctuations inherent in nanoscale characterization. SIMS depth profiling of lithium-implanted samples verified that a linear dose gradient was achieved across a single specimen.

These two techniques significantly enhance the flexibility and efficiency of ion irradiation experiments for fusion materials research. Their combined use enables systematic investigations of depth- and dose-dependent irradiation effects under well-controlled and reproducible conditions, while minimizing beam time and sample consumption.

CRediT authorship contribution statement

Mario Matić: Writing – review & editing, Writing – original draft, Visualization, Software, Methodology, Investigation, Formal analysis, Data curation, Conceptualization. **Toni Dunatov:** Writing – review & editing, Investigation, Formal analysis, Conceptualization. **Tonči Tadić:** Supervision. **Dmitry Terentyev:** Validation, Supervision. **Koray L. Iroc:** Writing – review & editing, Validation, Investigation. **Tatjana Filipič:** Validation, Investigation. **Janez Kovač:** Writing – review & editing, Validation, Supervision, Investigation.

Declaration of competing interest

The authors declare that they have no known competing financial interests or personal relationships that could have appeared to influence the work reported in this paper.

Acknowledgements

The authors acknowledge the support of the DiFU facility team at the Ruđer Bošković Institute. SIMS measurements were performed at the Department of Surface Engineering, Jožef Stefan Institute, Ljubljana. TEM and FIB preparation were carried out at SCK CEN, Mol.

This work has been carried out within the framework of the EUROfusion Consortium, funded by the European Union via the Euratom Research and Training Programme (Grant Agreement No 101052200 - EUROfusion). Views and opinions expressed are however those of the author(s) only and do not necessarily reflect those of the European Union or the European Commission. Neither the European Union nor the European Commission can be held responsible for them.

Data availability

Data will be made available on request.

References

[1] G. Was, Challenges to the use of ion irradiation for emulating reactor irradiation, J. Mater. Res. 30 (9) (2015) 1158–1182.
[2] S. Zinkle, L. Snead, Opportunities and limitations for ion beams in radiation effects studies: bridging critical gaps between charged particle and neutron irradiations, Scr. Mater. 143 (2018) 154–160.
[3] T. Tadic and others, "Development of the Dual-Beam Ion Irradiation Facility for Fusion Materials (DiFU)," *Materials,* vol. 16, 2023.
[4] L. Beck, Y. Serruys, S. Miro, P. Trocellier, E. Bordas, F. Lepretre, D. Brimbal, T. Loussouarn, H. Martin, S. Vaubaillon, S. Pellegrino, Ion irradiation and radiation effect characterization at the JANNUS-Saclay triple beam facility, J. Mater. Res. 30 (9) (2015) 1183–1194.
[5] S. Kurashima, T. Satoh, Y. Saitoh and W. Yokota, "Irradiation Facilities of the Takasaki Advanced Radiation Research Institute," *Quantum Beam Sci.,* vol. 1, 2017.
[6] S. Taller, F. Naab, G. Was, A methodology for customizing implantation profiles of light ions using a single thin foil energy degrader, Nucl. Instrum. Methods Phys. Res., Sect. B 478 (2020) 274–283.
[7] S. Taller, D. Woodley, E. Getto, A.M. Monterrosa, Z. Jiao, O. Toader, F. Naab, T. Kubley, S. Dwaraknath, G.S. Was, Multiple ion beam irradiation for the study of radiation damage in materials, Nucl. Instrum. Methods Phys. Res. B 412 (2017) 1–10.
[8] P. Sigmund, K.B. Winterbon, Energy and angular distributions of ions sputtered from solids, Nucl. Instrum. Methods 119 (1974) 541–549.

[9] G. Amsel, G. Battistig and A. L'Hoir, "Stopping power measurements in the MeV range," *Nucl. Instrum. Methods Phys. Res. B,* vol. 201, no. 325–332, 2003.

[10] A. Marwick, P. Sigmund, Sputtering yields of amorphous and polycrystalline targets, Nucl. Instrum. Methods 126 (1975) 317–323.

[11] J. Ziegler, M. Ziegler and J. Biersack, "SRIM – The stopping and range of ions in matter," vol. 268, p. 1818–1823, 2010.

[12] S. Gorondy-Novák, F. Jomard, F. Prima, H. Lefaix-Jeuland, SIMS as a new methodology to depth profile helium in as-implanted and annealed pure bcc metals? Nucl. Instrum. Methods Phys. Res. B 398 (2017) 56–64.

[13] C. Hardie, A. London and J. Lin, "Exploitation of thermal gradients for investigation of irradiation temperature effects with charged particles," *Sci. Rep.,* vol. 9, 2019.